ACS APPLIED ENERGY MATERIALS

www.acsaem.org Article

Effect on the Optical Efficiency and Photostability of Luminescent Solar Concentrator Based on the Deposition of $AgSiO_2$@NPs

Camilo Segura,* Víctor Vargas, Rodrigo A. Valenzuela-Fernández, Caroline Silva Danna, and Igor O. Osorio-Román*

Cite This: *ACS Appl. Energy Mater.* 2020, 3, 7680−7688 Read Online

ACCESS | Metrics & More | Article Recommendations | Supporting Information

ABSTRACT: Because of the growing demand for the use of photovoltaic cells to transform solar energy into electrical energy, radiation concentration systems such as luminescent solar concentrators (LSCs) have gained significant attention. This work presents an LSC system based on the effect of SiO_2-capped silver nanoparticles ($AgSiO_2$@NPs) on the optical efficiency of the LSC. For this purpose, $AgSiO_2$@NPs were deposited on a polymethylmethacrylate (PMMA) substrate using the layer-by-layer technique, and the luminescent material tetraphenylporphyrin (TPP) and Coumarin 6 were deposited by the spin-coating technique on a PMMA substrate with $AgSiO_2$@NPs. Then, the emission analysis of the two systems (PMMA/$AgSiO_2$@NPs/Coumarin 6 and PMMA/$AgSiO_2$@NPs/TPP) demonstrates that the nanoparticles enhanced fluorescence 20 and 8 times for TPP and Coumarin 6, respectively. Finally, the optical efficiency of the LSC was determined using a photodiode system. The results show an increase in optical efficiency because of two effects, the amplification of the luminescence and the dispersion caused by the nanoparticles, obtaining a maximum efficiency of 1.8 for our LSC system.

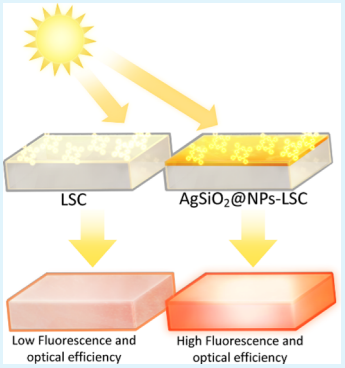

KEYWORDS: *luminescent solar concentrator, SEF, $AgSiO_2$@NPs, photostability, tetraphenylporphyrin, Coumarin 6*

1. INTRODUCTION

In recent decades, the use of energy from the sun as renewable energy has been growing, mainly conversion of solar energy into electrical energy through photovoltaic cells. However, given its high cost of production, alternatives have been sought to concentrate the light and thus reduce the size of the photovoltaic cells.[1] An alternative to the solar cell classic systems is the luminescent solar concentrator (LSC), which takes advantage of the luminescent properties of molecules or nanocrystals to concentrate the light. Its operation is based on the absorption of light by the molecule or nanocrystal that is inserted in a transparent matrix and then emits photons via luminescence. These photons are guided by multiple internal reflections and concentrated on the edge of the matrix.[2,3] A schematic representation of an LSC is shown in Figure 1. The ability of an LSC to concentrate sunlight is called optical efficiency and is determined by several factors.[4] One of these factors is the efficiency of photoluminescence, related to the ability of molecules or nanocrystals to emit light via luminescence, or their quantum yield.[5] Also, the optical efficient and the photostability of the molecules are independent parameters for the LSC system; hence, they must be evaluated separately. In this sense, it is desirable that the solar devices are made up of photostable molecules.[6,7]

Luminescent emission of a molecule or nanocrystal can be increased by the interaction with metallic nanoparticles, a process known as metal enhanced fluorescence (MEF),[8] surface-enhanced fluorescence (SEF),[9] or shell-isolated nanoparticle-enhanced fluorescence (SHINEF).[10] In MEF, SEF, and SHINEF, the most common nanoparticles used are silver and gold, and to be an effective process, the fluorophore must be at a nanometric distance greater than 2 nm from the nanoparticles. It is important to maintain this distance to avoid

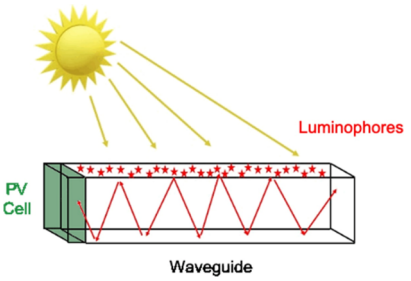

Figure 1. Schematic representation of LSC. Luminophores absorb radiation from the sun and emit photons via luminescence, which are transported by multiple internal reflections to the edge of the matrix (waveguide) and subsequently transformed into energy by the photovoltaic cell (PV cell).

Received: May 12, 2020
Accepted: July 22, 2020
Published: July 22, 2020

https://dx.doi.org/10.1021/acsaem.0c01094
ACS Appl. Energy Mater. 2020, 3, 7680−7688

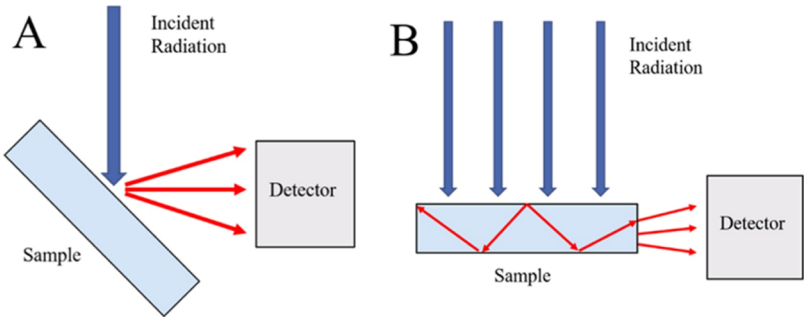

Figure 2. Scheme of measurement fluorescence (A) in front and (B) at the edge of the matrix.

deactivation of the excited state by the energy transfer process between fluorophores and nanoparticles.[11,12] An alternative for this separation is to cap the nanoparticles with different types of compounds such as amines,[13,14] carboxylates,[15,16] thiols,[17] and SiO_2.[18,19]

Recent papers have reported enhanced fluorescence in the LSC system using silver and gold nanoparticles,[20−26] that increase the effect up to 24-fold. However, the previous reports have not studied the effect of the separation distance between metal nanoparticles with SiO_2-capped and fluorophores in LSC systems. In addition, the use of fluorophores with high quantum yields, which generally produce low enhanced luminescence, was reported in literature.[27]

The main goal of this work is to determine the effect on the optical efficiency in LSC systems with TPP and Coumarin 6, molecules that have different photophysical properties, and the role that SEF of those fluorophores would play on the optical efficiency.

2. EXPERIMENTAL SECTION

2.1. Materials. A piece of 22 × 22 × 2 mm of polymethylmethacrylate (PMMA) was used as a matrix. PMMA pieces were purchased from Polymershapes S.A. Chile. The luminophores employed were tetraphenylporphirine (TPP) and Coumarin 6 (both from Sigma-Aldrich). Solutions of luminophores were prepared in chloroform (Sigma Aldrich) and polyvinylformion (FORMVAR, Sigma-Aldrich). $AgNO_3$ (Sigma-Aldrich) and tetraethylortisilicate (TEOS, Sigma-Aldrich) were used to synthetize silver nanoparticles (AgNPs) capped with SiO_2.

2.2. Synthesis of AgNPs. The synthesis of AgNPs is based on protocols described by Lee−Mesiel.[28] $AgNO_3$ (18 mg) was dissolved in 100 mL of Milli-Q water and the solution was brought to boil; at this point, 2 mL of trisodium citrate (38.8 mM) was added into it. This solution was boiled for 1 h and let to cool down at room temperature to obtain a colloidal suspension of AgNPs, which was centrifuged for 10 min at 1000 rpm. The supernatant was collected for the next step.

2.3. Formation of AgNp Capped with SiO_2 ($AgSiO_2$@NPs).[29] For silver coating, 9 mL of colloidal suspension was added into 40 mL of ethanol. To this solution, 1.25 mL of ammonia 30 % wt and 40 μL of TEOS (40 mM) were added. The solution was agitated for 2 min and allowed to settle down for 48 h. After 48 h, the solution was centrifuged for 45 min at 5000 rpm, and the precipitate was collected and dispersed in water.

2.4. $AgSiO_2$@NPs Deposition on the PMMA Matrix. The deposition of $AgSiO_2$@NPs on the PMMA matrix was carried out through the layer-by-layer methodology, taking advantage of the fact that the $AgSiO_2$@NPs have a negative surface charge density.[30] This allows the $AgSiO_2$@NPs to adsorb on the surface. The PMMA matrix was submerged into a solution of NaOH (1 M) for 1 h. Then, the matrix was brought to a solution of polydiallyldimethylammonium chloride (1% wt) for 30 min. Finally, the matrix was introduced to the colloidal solution of $AgSiO_2$@NPs for 12 h.

2.5. Molecules Deposition on the PMMA−$AgSiO_2$@NPs Matrix. The molecules used in this study were TPP and Coumarin 6, which were dissolved in a solution of FORMVAR 0.01% in chloroform. The polymer creates a thin film on the PMMA matrix, and this protected the molecules deposited by spin coating. Deposition of molecules was realized by spin coating at 2000 rpm for 1 min. The volume added were 50 μL of each molecule, and the concentration of the solutions varied from 5×10^{-4} to 1×10^{-3} M.

2.6. Characterization. The UV−visible studies were carried out using a Shimadzu UV-1800 spectrophotometer. The fluorescence spectrophotometer ISS PC1 was used to measure the fluorescence intensity. The excitation of TPP was realized with a xenon arc lamp at 420 and 514 nm, while the excitation of Coumarin 6 was realized with a laser of 445 nm. Fluorescence spectra were measured in the front and in the border of the PMMA matrix. Additionally, because of the optical nature of the LSC system, it is important to perform the measurement of the emission, at the front and the edge of the matrix. A schematic representation of this measurement is shown in Figure 2.

Lifetime measurement of the luminophores was performed with a Lifetime II instrument. The study of the size of nanoparticles and the thickness of the SiO_2 layer, was performed by transmission electron microscopy (Hitachi HT7700 TEM). Atomic force microscopy (WiTec Alpha 3000) was used to determinate the distribution of $AgSiO_2$@NPs on the PMMA matrix, using a 75 kHz tip.

2.7. Optical Efficiency. To measure the optical efficiency of LSC, an apparatus proposed by Carlotti[31] was build (see Figure S1 at the Supporting Information). In this case, the Solar simulator SS150 Sciencetech AAA class was used, which is equipped with an air/mass filter 1.5. The detection system consists of five OSRAM photodiodes connected in parallel with active area 2.7 × 2.7 mm and high response in the visible spectrum (400−1100 nm). The current generated by the photodiodes was measured using the multimeter Keithley 2400.

3. RESULTS AND DISCUSSION

3.1. Characterization of AgNPs and $AgSiO_2$@NPs. The SiO_2 coated around AgNPs is used as a spacer between fluorophores and nanoparticles to avoid the deactivation of the excited state by the energy transfer process between fluorophore−nanoparticle and so obtained SEF. Figure 3A shows the extinction spectra of AgNPs and $AgSiO_2$@NPs. It is possible to observed that the spectrum of $AgSiO_2$@NPs presents a redshift because of silica coating. This occurs because of the dielectric constant surrounding the nanoparticles changes.[32,33] The TEM image observed in Figure 3B confirms that the $AgSiO_2$@NPs are coated.[34,35] The nanoparticles diameter is 65.0 ± 6.5 nm and surrounding the AgNPs is a layer with 5.0 ± 1.0 nm thickness (see Figures 3C and S2).

The Figure 4A shows the extinction spectrum of $AgSiO_2$@NPs deposited on the PMMA matrix and the comparison with the extinction spectrum of $AgSiO_2$@NPs in a colloidal solution. A blueshift of the resonance plasmon, from 431 to

https://dx.doi.org/10.1021/acsaem.0c01094
ACS Appl. Energy Mater. 2020, 3, 7680−7688

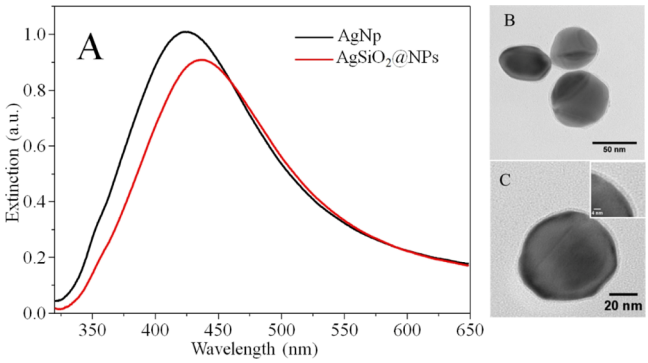

Figure 3. (A) Extinction spectra of AgNPs and $AgSiO_2$@NPs (B,C) TEM image of $AgSiO_2$@NPs.

418 nm, was observed; this change is a response to the variance in the refractive index of the medium that surrounds the nanoparticles.

In this sense, Figure 4B shows a Mie theory calculation to corroborate the effect previously cited,[36] the extinction spectrum for a 65.0 nm diameter nanoparticle, with a 5.0 nm coat layer of silica, shows a similar shift, when nanoparticles change from water to air. For that reason, these results endorse that the spectrum shift is not related to a change in the structure of $AgSiO_2$@NPs, but it is a consequence of the variance in the dielectric constants of the medium that surrounds the nanoparticles as mentioned in the previous paragraph.

Figure 5A shows the AFM image of $AgSiO_2$@NPs that was transferred to the PMMA surface, and it is possible to observe that the nanoparticles are separated from each other, and the coating does not allow their aggregation in solid. Figure 5B shows the AFM of the Ag nanoparticles without SiO_2 in PMMA and the aggregation of these nanoparticles is clearly noticed (see the yellow square). Additionally, the bottom of the AFM images shows height profiles, and it could be discerned that (i) nanoparticles without coated are smaller than the coated ones and (ii) nanoparticles with SiO_2 have a height profile, similar in size to the observed in the images of TEM.

Consequently, it is important to remark that the process of transferring the coated nanoparticles to the PMMA matrix does not change or damage the SiO_2 coating. In this sense, this result is corroborated by the resonance plasmon spectra from Figure 4A. The extinction spectrum maintained a similar shape and only a blue shift was observed, indicating that the $AgSiO_2$@NPs are intact on the surface of the PMMA matrix.

3.2. SEF by $AgSiO_2$@NPs. Analyzing the Figure 6, for the TPP, a typical one Soret band at 420 nm and four Q-bands at 514, 548, 591, and 646 nm in the absorption spectrum and two emission peaks at 650 and 717 nm in the emission spectrum, respectively, are observed. The Coumarin 6 shows a band with two peaks at 446 and 466 nm in the absorption spectra and one emission with a maximum at 508 nm. The absorbance and emission spectra were recorded for TPP and Coumarin 6 on PMMA and are shown in Figures S3 and S4 (Supporting Information).

The spectral overlap with the plasmon resonance of the nanoparticle and the molecules is one of the important factors which determines SEF.[37−39] Figure 6 shows the overlap of the plasmon resonance of the $AgSiO_2$@NPs with TPP and Coumarin 6, and we observe a considerable overlap between the absorbances and the extinction spectrum. In this sense, if excited-state fluorophores are an overlap with near-field from metal nanoparticles (plasmon) and a optimized distance from the nanoparticles, the fluorophore-induced by the plasmons is able to emit to the far-field and observable as surface-enhanced emission. In this sense, our systems fulfill this condition, therefore, it was possible to observe enhanced emissions for TPP and Coumarin 6.

The SEF spectra were measurement at 420 and 514 nm excitation wavelengths for TPP and 445 nm excitation wavelength for Coumarin 6. Enhanced factors (EF) were calculated using the eq 1

$$\mathrm{EF} = \frac{I_{\mathrm{np}}}{I_{\mathrm{f}}} \tag{1}$$

Thus, I_{np} is the total intensity of emission spectra in the presence of nanoparticles and I_{f} is the total intensity of emission spectra without nanoparticles. Table 1 shows the amplification factors of TPP and Coumarin 6 measured at the front and at the edge of the matrix. All emission spectra for the calculation of the amplification factor are shown in the Supporting Information (Figures S5−S7). The study of the emission at the front and at the edge of the matrix is necessary to evaluate the path of the emission into the matrix.

In general, Table 1 shows that TPP has greater EF than the Coumarin 6 samples. According to the literature, the values of the enhanced factor present the same tendency as amplified fluorescence studies in solution, and is evident that the photophysical properties play a important role in the enhanced factor of SEF.[40−43]

An important result shown in Table 1 is the comparison between the amplification factors when the emission is

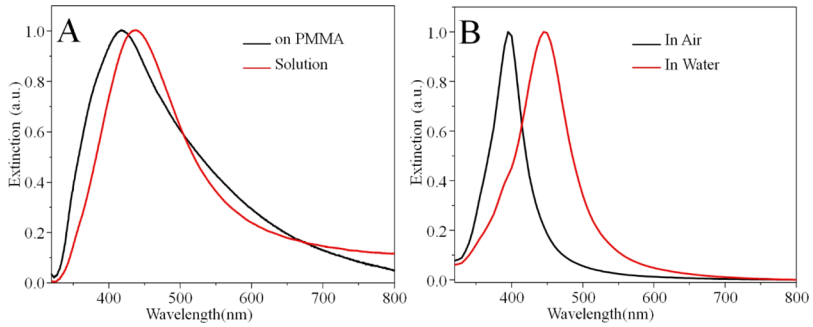

Figure 4. (A) Extinction spectrum of $AgSiO_2$@NPs in solution and deposited on PMMA and (B) Mie theory calculation of extinction cross sectional area of $AgSiO_2$@NPs in water and air.

https://dx.doi.org/10.1021/acsaem.0c01094
ACS Appl. Energy Mater. 2020, 3, 7680−7688

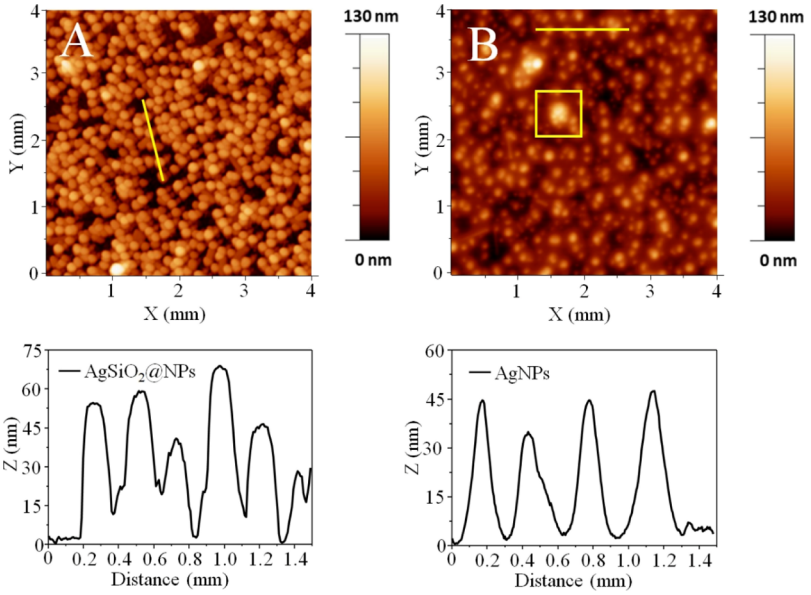

Figure 5. (A) AFM image of $AgSiO_2$@NPs deposited on PMMA. (B) AFM image of Ag NPs deposited on PMMA. AFM height profiles for the corresponding lines drawn in images A and B (yellow line).

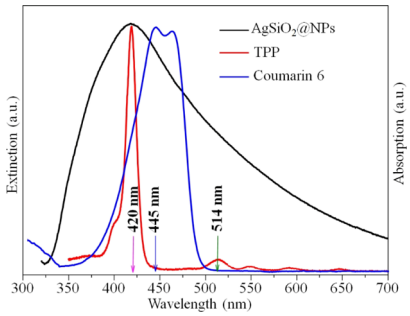

Figure 6. Overlap of the extinction spectrum of $AgSiO_2$@NPs and absorbance spectra of TPP and Coumarin 6.

Table 1. Amplification Factor of TPP and Coumarin 6 on the Side and Edge of LSC

	EF on the front		EF on the edge	
	Exc 420 nm	Exc 514 nm	Exc 420 nm	Exc 514 nm
PMMA−$AgSiO_2$@NPs−TPP	5.1	19	2.8	10
		Exc 445 nm		Exc 445 nm
PMMA−$AgSiO_2$@NPs−Coumarin 6		11		2.0

measured at the front and at the edge of the sample. It is observed that for both TPP and Coumarin 6, the amplification is greater when measured at the front of the sample. This amplification it is probably observed because of a part of the photons emitted by the luminescent molecules are not being transmitted through the matrix and does not reach the edges of the LSC; the reasons for this event could be the follows: (i) the photons emitted from the molecules escape from the matrix, (ii) self-absorption photons in the solid sample, and (iii) related to the surface roughness, which, as seen in the AFM image, is not smooth.

Furthermore, the results associated with TPP molecules are interesting, while Coumarin 6 has average amplification values of 11 and 2, at the front and at the edge, respectively. The TPP molecules change their amplification factor for both (front and edge) when we change the excitation wavelength. Interestingly, under the same experimental conditions, the fluorescence of TPP increases up to 3.5 times when using 514 nm than 420 nm as the excitation wavelength, resulting in the modification of the enhanced factor for TPP. In this sense, Klem and Waluk[44] and Kim et al.[45] describe this phenomenon for TPP in the presence of silica-coated gold nanoparticles using theoretical and experiment data. The TPP molecules presents an unusual SEF behavior, that is, their enhanced fluorescence gradually increases when the wavelength used for TPP excitation moves from the Soret band to the Q-bands (redshift). These results corroborate the values presented in our work in Table 1. Besides, Kim et al. report that the optimal distance between the TPP and the metal is between 2 and 11 nm; hence, the nanoparticle coating thickness of 5 nm used in this work is suitable for SEF studies.[45]

On the other hand, the spectral overlap at 420 nm is higher than at 514 nm, but experimentally we observed an upper enhanced factor when the excitation wavelength was at 514 nm, and this result clearly indicated that SEF of the TPP is depend on the plasmon effect (near-field) and the absorption wavelengths of fluorophores.[19,46] In the case of TPP, different absorbance coefficients in the molecular system, could be another control factor of the enhanced fluorescence and probably in the enhanced optical efficient of the LSC system.

3.3. Lifetime TPP and Coumarin 6. In classical fluorescence experiments, the changes in quantum yields and lifetimes are due to changes in the nonradiative decay rates k_{nr}, which result from changes in a fluorophore's environment, quenching, or Förster resonance energy transfer.[40,47] When a nanoparticle interacts with a fluorophore, the lifetimes are given by the following equation[43]

$$\tau_m = \frac{1}{\Gamma + \Gamma_m + k_{nr}} \quad (2)$$

where τ_m is the lifetime in the presence of nanoparticles, Γ is the radiative deactivation constant, Γ_m is the radiative deactivation in the presence of nanoparticles, k_{nr} is the nonradiative deactivation constant in the presence of $AgSiO_2$@

https://dx.doi.org/10.1021/acsaem.0c01094
ACS Appl. Energy Mater. 2020, 3, 7680−7688

NPs. The nanoparticles decrease the lifetimes and increase the emission, and this is a unique spectral change for fluorophores near the metal nanoparticles or metal surfaces.[40,47]

Table 2 shows the average lifetimes for both molecules TPP and Coumarin 6, and the time-correlated single-photon counting values obtained for these molecules are shown in the Supporting Information, Figures S8 and S9 and Tables S-1 and S-2.

Table 2. Average Lifetime of TPP and Coumarin 6 on PMMA and PMMA−$AgSiO_2$@NPs.

samples	$\langle\tau\rangle$ (ns)
PMMA−TPP	9.78
PMMA−$AgSiO_2$@NPs−TPP	4.85
PMMA−Coumarin 6	3.22
PMMA−$AgSiO_2$@NPs−Coumarin 6	1.72

The values summarized in Table 2 shows that both molecules present a decrease in lifetime by interacting with the nanoparticles. This is a typical effect when fluorophores interact with metal nanoparticles and values are agreed with the literature.[27,48,49]

In this study, the fluorophores (TPP and Coumarin 6) in the presence of $AgSiO_2$@NPs not only has the normal deactivation channel of the free molecule, but also, a new deactivation process from the excited-state are generated because of the coupling between the molecule and near-field from plasmon, resulting in an enhance fluorescence and decreasing the lifetime of excitation state of the fluorophore, which leads to the conclusion that the emitting system is the fluorophore−nanoparticle couple. Therefore, if the system experiences more deactivations process, mathematically, more terms in the denominator of eq 2 will be added, resulting in a shorter lifetime[40,47,50] leading to photobleaching decrease.

Our results for surface enhanced-fluorescence and the lifetime excitation state agree with the literature and the theoretical concepts described above (see Figures S5−S7 and in Tables S-1 and S-2). Additionally, to the shorter lifetime, the presence of $AgSiO_2$@NPs could change the molecule photostability in terms of photobleaching. The photobleaching is the photochemical destruction of a fluorophore in an excited state. Therefore, a decreased lifetime should allow the fluorophore to undergo more excitation−deexcitation cycles prior to the photobleaching process.[51−53]

3.4. Study of Photostability (Photobleaching). The stability of the fluorophore was evaluated by the variation of the emission intensity of the samples with TPP and Coumarin 6 with and without $AgSiO_2$@NPs over time. The excitation wavelength of TPP was 420 nm while for Coumarin, 6, 445 nm; the intensity of emission was measured at 508 nm for Coumarin 6 and 650 nm for TPP.

The Figure 7 shows normalized fluorescence intensity versus time, for both experiments, for 170 min.

The data in Figure 7 indicate an increase in the fluorescence intensity of both molecules in the presence of $AgSiO_2$@NPs. This result is expected because of the decrease in the lifetime of the molecules, indicating a better molecule photostability over time, and consequently, could improve the LSC system permitting a long exposure times to solar radiation.

In other words, the normalized intensity for Coumarin 6 with $AgSiO_2$@NPs decrease a 13% from 1.0 until 0.87 in 170 min, while TPP decreases rapidly, in two steps; first from 1.0 to 0.50 in the first 20 min, and then reach a constant value of 0.35 in 160 min, corresponding to a decrease of 65%.

3.5. Optical Efficiency of LSC (% η_{opt}). The ability of an LSC to concentrate sunlight is called optical efficient, and as mentioned in the introduction, photoluminescence or luminescence is one of the determining factors to the efficiency of the LSC system because of total internal reflection of the re-emitted light, which is waveguided to the edges for conversion to electricity.

The optical efficiency is defined as

$$\%\,\eta_{opt} = \frac{I_{LSC}}{I_{SC} \times G} \times 100 \tag{3}$$

$$G = \frac{A_{top}}{A_{edge}} \tag{4}$$

where I_{LSC} is the current measured at the edge of LSC, I_{SC} the measured current from the photodiodes under direct illumination by the radiation source, A_{top} is the area exposed to the radiation of LSC and A_{edge} is the edge area of LSC, the value of A_{edge} is multiple by 4 (number of the edges of the PMMA matrix); all the currents were measurement with the solar simulator SS150 Sciencetech AAA. The G value is 2.75 and I_{SC} is 6.50 mA (6500 μA). Further, different samples with concentrations of fluorophores were prepared to study the effect of this parameter on optical efficiency.

Tables 3 and 4 shown the values of optical efficiency (% η_{opt}) for different fluorophore concentration of TPP and Coumarin 6, respectively. The currents were measurement in microampere (μA), the source of illumination is the solar simulator (see Figure S1, Supporting Information). Additionally, the Figure 8 show a photograph of the LSCs built with and without $AgSiO_2$@NPs, exposed to the sun light.

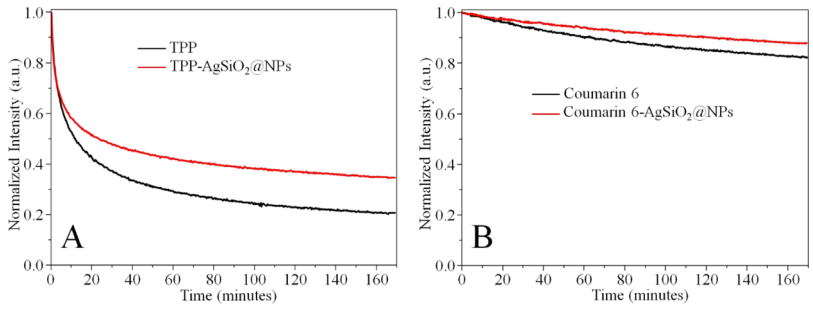

Figure 7. Intensity profile over time and the change in photostability, i.e., produced by $AgSiO_2$@NPs. (A) TPP. (B) Coumarin 6.

https://dx.doi.org/10.1021/acsaem.0c01094
ACS Appl. Energy Mater. 2020, 3, 7680−7688

Table 3. LSC Photocurrent (Pc) for TPP with and without Nanoparticles for Different Concentrations

molar concentration (M)	TPP[a] Pc (μA)	NPs−TPP[b] Pc (μA)	% η_{opt} [c]	% η_{opt} [d]
5.0×10^{-4}	2.0	235.0	0.01	1.32
1.0×10^{-3}	5.3	260.0	0.03	1.46
5.0×10^{-3}	8.0	290.0	0.05	1.62
1.0×10^{-2}	9.0	285.0	0.05	1.60

[a]PMMA−TPP. [b]PMMA−$AgSiO_2$@NPs−TPP. [c]Optical efficiency without nanoparticles. [d]Optical efficiency with nanoparticles.

Table 4. LSC Photocurrent (Pc) for Coumarin 6 with and without Nanoparticles for Different Concentrations

molar concentration (M)	C6[a] Pc (μA)	NPs-C6[b] Pc (μA)	% $\eta_{opt\ 1}$ [c]	% $\eta_{opt\ 2}$ [d]
5.0×10^{-4}	5.0	240.0	0.03	1.34
1.0×10^{-3}	13.7	280.0	0.08	1.57
5.0×10^{-3}	19.7	317.0	0.11	1.77
1.0×10^{-2}	21.8	328.0	0.12	1.84

[a]PMMA−Coumarin 6. [b]PMMA−$AgSiO_2$@NPs−Coumarin 6. [c]Optical efficiency without nanoparticles. [d]Optical efficiency with nanoparticles.

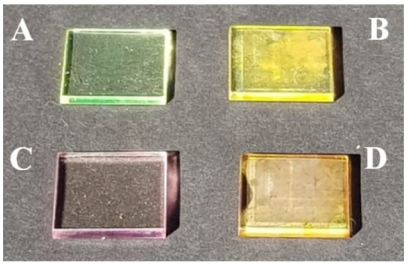

Figure 8. LSC built with and without $AgSiO_2$@NPs. On the left are those without $AgSiO_2$@NPs [Coumarin 6 (A) and TPP (C)] and on the right those with $AgSiO_2$@NPs [Coumarin 6 (B) and TPP (D)].

The results from Tables 3 and 4 showed two important effects: (i) the concentration of fluorophores increases leading to a current increment and (ii) the fluorophores with nanoparticle generate an increase in the current when compared to the values of the fluorophores without nanoparticles; this effect was observed for both, TPP and Coumarin 6. Consequently, these two effects are seen clearly when calculating the optical efficiency considering the system with and without nanoparticles. In this sense, the optical efficiency, considering just the photons from the fluorophore (emission without nanoparticles), has a maximum value of 0.05 and 0.12% for TPP and Coumarin 6, respectively, while for the samples with SEF, the values were 1.60% for TPP and 1.84% for Coumarin 6.

Therefore, the nanoparticles permitted an increase in the optical efficiency, shown in Figure 9A, and for both fluorophores, the optical efficiency increases until it reaches a constant value. In this point is important to note that the data shown in Figure 9A and Tables 3 and 4 represent the whole values, that is, without discounting the background of the sample.

The background is considering as a current in the absence of fluorophores, in other words, the current evaluation was performed in samples with PMMA−$AgSiO_2$@NPs and generated an average current is 195 μA. This amount is correlated with the scattering of the PMMA−$AgSiO_2$@NPs. Hereupon, Figure 9B shows a comparative to the optical efficiency, discounting the background for the system, and will be discussed ahead.

Particularly, Coumarin 6 has a better performance in optical efficiency for both systems, with and without nanoparticles, comparing to the TPP samples. Initially, the higher SEFs enhanced factor of TPP could induce to consider that this system will have better optical efficiency than Coumarin 6, conversely, the information provided in this paper establish that the Coumarin 6 has an optical efficiency and it allows to conclude that Coumarin 6 is a better candidate to be used in our LSC system.

The results observed in Figure 9B, discounting the scattering,[54] have a tendency similar to those seen in Figure 9A, but the optical efficiency is reduced. The reduction in this parameter leads to conclude that the background has an important impact on the optical efficiency, for this reason, the contribution of the interaction between light and nanoparticles should be considered and evaluated in the global analysis for the LSC system in future investigations.[54]

Finally, comparing our system with those published in the literature,[55,56] perhaps the amounts are below to the maximum optical efficiency values reported; but it is important to consider that the systems proposed here use thin film with a low amount of material (fluorophore−metal nanoparticles) to develop an LSC device, influencing the cost of the device, which could convert windows of the house and/or building into an LSC system with a low amount of material. In this

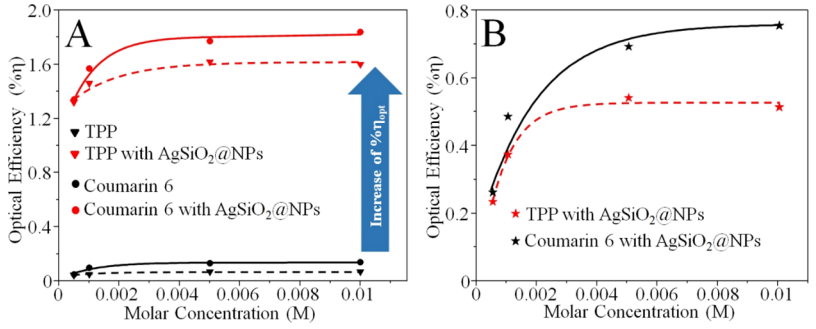

Figure 9. (A) Optical efficiency for LSC and its dependence with the concentration of fluorophores. Triangle points (black and red) correspond to TPP data, and circle points (black and red) correspond to Coumarin 6 data. (B) Optical efficiency for LSC and its dependence with the concentration of fluorophores without background. Star (red) correspond to TPP data, and star (black) correspond to Coumarin 6 data. All of the points were fitted to an exponential curve.

https://dx.doi.org/10.1021/acsaem.0c01094
ACS Appl. Energy Mater. 2020, 3, 7680−7688

sense, the idea is to continue modifying other elements of the LSC system to obtained better results as (i) different polymeric matrices,[57,58] (ii) other organic and inorganic dyes,[59,60] (iii) the effect of light scattering from the nanoparticles, (iv) photostability associated to the photobleaching process,[51−53] (iv) change the size and shape of the AgNPs[46] and (v) change the aggregation of the AgNPs,[61] inter alia, it could be futures projects to enhance the optical efficiency of the LSC system.

4. CONCLUSIONS

To begin with, the LSC systems with TPP and Coumarin 6 were analyzed and as a conclusion, the SEF and the scattering of the $AgSiO_2$@NPs are responsible to increase the optical efficiency in both systems. Furthermore, a molecular system such as TPP presents an unusual property in the presence of $AgSiO_2$@NPs associated with the excitation wavelength and a better SEF, when compared to the Coumarin 6; however, Coumarin 6 has better optical efficiency results and less photobleaching.

According to SEF, results the shell-isolated AgNPs ($AgSiO_2$@NPs) in an LSC allow the maximum amplification of the fluorescent of TPP and Coumarin 6 of 20-fold and eightfold, respectively. In addition, $AgSiO_2$@NPs produce an effect of dispersion of the incident radiation that is added to the fluorescence of the molecules, affecting the optical efficiency of the LSC.

On the one hand, SEF could be a key to control the optical efficiency of the LSC system; however, the photostability of the molecule plays an important role as well in the management of the LSC parameters. Finally, the concentration of TPP and Coumarin 6, increases the current in the system and leads to greater optical efficiency until reaching a constant value.

In conclusion, the combination of Coumarin 6 and $AgSiO_2$@NPs is an advantageous option to use in an LSC considering the molecule photostability, the SEF, and the optical efficiency.

■ ASSOCIATED CONTENT

Supporting Information

The Supporting Information is available free of charge at https://pubs.acs.org/doi/10.1021/acsaem.0c01094.

Device used for LSC measurement, TEM images, absorption and emission spectra, decay profiles of the excited state of TPP and Coumarin 6 with and without $AgSiO_2$@NPs, and LSC measurement system (PDF)

■ AUTHOR INFORMATION

Corresponding Authors

Camilo Segura − *Departamento de Química, Facultad de Ciencias, Universidad de Chile, Santiago 7800003, Chile;* orcid.org/0000-0003-1091-5397; Email: camilo.segura@ug.uchile.cl

Igor O. Osorio-Román − *Centro de Nanotecnología Aplicada, Facultad de Ciencias and Núcleo de Química y Bioquímica, Facultad de Estudios Interdisciplinarios, Universidad Mayor, Santiago 8580745, Chile;* orcid.org/0000-0001-7502-8698; Email: igor.osorior@gmail.com, igor.osorio@umayor.cl

Authors

Víctor Vargas − *Departamento de Química, Facultad de Ciencias, Universidad de Chile, Santiago 7800003, Chile;* orcid.org/0000-0002-5126-6699

Rodrigo A. Valenzuela-Fernández − *Departamento de Química, Facultad de Ciencias, Universidad de Chile, Santiago 7800003, Chile;* orcid.org/0000-0001-5071-7630

Caroline Silva Danna − *Departamento de Física, Facultad de Ciencias, Universidad de Santiago de Chile, Santiago 9170124, Chile;* orcid.org/0000-0001-8188-9419

Complete contact information is available at: https://pubs.acs.org/10.1021/acsaem.0c01094

Author Contributions

The manuscript was written through equal contributions of all authors and them have given approval to the final version of the manuscript.

Notes

The authors declare no competing financial interest.

■ ACKNOWLEDGMENTS

C.S. was supported by PhD CONICYT project no. 21150397. I.O.O.-R. acknowledge to FONDECYT (Fondo Nacional de Desarrollo Científico y Tecnológico) project no. 1190246. All authors acknowledge to CONICYT project EQM140142 (Fondo de Equipamiento Científico y Tecnológico, FONDEQUIP) and the Laboratorio de Química Biosupramulecular of Pontificia Universidad Católica de Chile for the use of the LifeSpec II spectrometer for the determination of lifetimes.

■ REFERENCES

(1) Swanson, R. M. Promise of Concentrators. *Prog. Photovoltaics Res. Appl.* **2000**, *8*, 93−111.

(2) Debije, M. G.; Verbunt, P. P. C. Thirty Years of Luminescent Solar Concentrator Research: Solar Energy for the Built Environment. *Adv. Energy Mater.* **2012**, *2*, 12−35.

(3) Hermann, A. M. Luminescent Solar Concentrators-A Review. *Sol. Energy* **1982**, *29*, 323−329.

(4) Goetzberger, A.; Greubel, W. Solar Energy Conversion with Fluorescent Collectors. *Appl. Phys.* **1977**, *14*, 123.

(5) Goldschmidt, J. C.; Peters, M.; Prönneke, L.; Steidl, L.; Zentel, R.; Bläsi, B.; Gombert, A.; Glunz, S.; Willeke, G.; Rau, U. Theoretical and Experimental Analysis of Photonic Structures for Fluorescent Concentrators with Increased Efficiencies. *Phys. Status Solidi A* **2008**, *205*, 2811−2821.

(6) Zhang, Y.; Liu, X.; Osburn, C. L.; Wang, M.; Qin, B.; Zhou, Y. Photobleaching Response of Different Sources of Chromophoric Dissolved Organic Matter Exposed to Natural Solar Radiation Using Absorption and Excitation-Emission Matrix Spectra. *PLoS One* **2013**, *8*, No. e77515.

(7) Zaiba, S.; Lerouge, F.; Gabudean, A.-M.; Focsan, M.; Lermé, J.; Gallavardin, T.; Maury, O.; Andraud, C.; Parola, S.; Baldeck, P. L. Transparent Plasmonic Nanocontainers Protect Organic Fluorophores against Photobleaching. *Nano Lett.* **2011**, *11*, 2043−2047.

(8) Geddes, C. D.; Lakowicz, J. R. Editorial: Metal-Enhanced Fluorescence. *J. Fluoresc.* **2002**, *12*, 121−129.

(9) Fort, E.; Grésillon, S. Surface Enhanced Fluorescence. *J. Phys. D: Appl. Phys.* **2008**, *41*, 013001.

(10) Guerrero, A. R.; Aroca, R. F. Surface-Enhanced Fluorescence with Shell-Isolated Nanoparticles (SHINEF). *Angew. Chem., Int. Ed.* **2011**, *50*, 665−668.

(11) Ray, K.; Badugu, R.; Lakowicz, J. R. Distance-Dependent Metal-Enhanced Fluorescence from Langmuir-Blodgett Monolayers of Alkyl-NBD Derivatives on Silver Island Films. *Langmuir* **2006**, *22*, 8374−8378.

(12) Swierczewska, M.; Lee, S.; Chen, X. The Design and Application of Fluorophore-Gold Nanoparticle Activatable Probes. *Phys. Chem. Chem. Phys.* **2011**, *13*, 9929−9941.
(13) Chen, M.; Feng, Y.-G.; Wang, X.; Li, T.-C.; Zhang, J.-Y.; Qian, D.-J. Silver Nanoparticles Capped by Oleylamine: Formation, Growth, and Self-Organization. *Langmuir* **2007**, *23*, 5296−5304.
(14) Marchetti, B.; Joseph, Y.; Bertagnolli, H. Amine-Capped Gold Nanoparticles: Reaction Steps during the Synthesis and the Influence of the Ligand on the Particle Size. *J. Nanopart. Res.* **2011**, *13*, 3353−3362.
(15) Wang, W.; Chen, X.; Efrima, S. Silver Nanoparticles Capped by Long-Chain Unsaturated Carboxylates. *J. Phys. Chem. B* **1999**, *103*, 7238−7246.
(16) Yamamoto, M.; Kashiwagi, Y.; Nakamoto, M. Size-Controlled Synthesis of Monodispersed Silver Nanoparticles Capped by Long-Chain Alkyl Carboxylates from Silver Carboxylate and Tertiary Amine. *Langmuir* **2006**, *22*, 8581−8586.
(17) Shimmin, R. G.; Schoch, A. B.; Braun, P. V. Polymer Size and Concentration Effects on the Size of Gold Nanoparticles Capped by Polymeric Thiols. *Langmuir* **2004**, *20*, 5613−5620.
(18) Kobayashi, Y.; Correa-duarte, M. A.; Liz-Marzán, L. M. Sol - Gel Processing of Silica-Coated Gold Nanoparticles. *Langmuir* **2001**, *17*, 6375−6379.
(19) Guerrero, A. R.; Zhang, Y.; Aroca, R. F. Experimental Confirmation of Local Field Enhancement Determining Far-Field Measurements with Shell-Isolated Silver Nanoparticles. *Small* **2012**, *8*, 2964−2967.
(20) El-Bashir, S. M.; Barakat, F. M.; Alsalhi, M. S. Metal-Enhanced Fluorescence of Mixed Coumarin Dyes by Silver and Gold Nanoparticles: Towards Plasmonic Thin-Film Luminescent Solar Concentrator. *J. Lumin.* **2013**, *143*, 43−49.
(21) El-Bashir, S. M.; Barakat, F. M.; AlSalhi, M. S. Double Layered Plasmonic Thin-Film Luminescent Solar Concentrators Based on Polycarbonate Supports. *Renewable Energy* **2014**, *63*, 642−649.
(22) Levchenko, V.; Grouchko, M.; Magdassi, S.; Saraidarov, T.; Reisfeld, R. Enhancement of Luminescence of Rhodamine B by Gold Nanoparticles in Thin Films on Glass for Active Optical Materials Applications. *Opt. Mater.* **2011**, *34*, 360−364.
(23) Reisfeld, R.; Pietraszkiewicz, M.; Saraidarov, T.; Levchenko, V. Luminescence Intensification of Lanthanide Complexes by Silver Nanoparticles Incorporated in Sol-Gel Matrix. *J. Rare Earths* **2009**, *27*, 544−549.
(24) Levchenko, V. Luminescence of Europium Complex Enhanced by Surface Plasmons of Gold Nanoparticles for Possible Application in Luminescent Solar Concentrators. *J. Lumin.* **2018**, *193*, 5−9.
(25) Sethi, A.; Chandra, S.; Ahmed, H.; McCormack, S. Broadband Plasmonic Coupling and Enhanced Power Conversion Efficiency in Luminescent Solar Concentrator. *Sol. Energy Mater. Sol. Cells* **2019**, *203*, 110150.
(26) Mateen, F.; Oh, H.; Jung, W.; Binns, M.; Hong, S.-K. Metal Nanoparticles Based Stack Structured Plasmonic Luminescent Solar Concentrator. *Sol. Energy* **2017**, *155*, 934−941.
(27) Dragan, A. I.; Geddes, C. D. Metal-Enhanced Fluorescence: The Role of Quantum Yield, Q0, in Enhanced Fluorescence. *Appl. Phys. Lett.* **2012**, *100*, 093115.
(28) Lee, P. C.; Meisel, D. Adsorption and Surface-Enhanced Raman of Dyes on Silver and Gold Sols. *J. Phys. Chem.* **1982**, *86*, 3391−3395.
(29) Liu, S.; Zhang, Z.; Han, M. Gram-Scale Synthesis and Biofunctionalization of Silica-Coated Silver Nanoparticles for Fast Colorimetric DNA Detection. *Anal. Chem.* **2005**, *77*, 2595−2600.
(30) Shanthil, M.; Thomas, R.; Swathi, R. S.; George Thomas, K. Ag@SiO_2 Core−Shell Nanostructures: Distance-Dependent Plasmon Coupling and SERS Investigation. *J. Phys. Chem. Lett.* **2012**, *3*, 1459−1464.
(31) Carlotti, M.; Fanizza, E.; Panniello, A.; Pucci, A. A Fast and Effective Procedure for the Optical Efficiency Determination of Luminescent Solar Concentrators. *Sol. Energy* **2015**, *119*, 452−460.
(32) Mie, G. Beiträge Zur Optik Trüber Medien, Speziell Kolloidaler Metallösungen. *Ann. Phys.* **1908**, *330*, 377−445.
(33) Kelly, K. L.; Coronado, E.; Zhao, L. L.; Schatz, G. C. The Optical Properties of Metal Nanoparticles: The Influence of Size, Shape, and Dielectric Environment. *J. Phys. Chem. B* **2003**, *107*, 668−677.
(34) Chou, K.-S.; Chen, C.-C. Fabrication and Characterization of Silver Core and Porous Silica Shell Nanocomposite Particles. *Microporous Mesoporous Mater.* **2007**, *98*, 208−213.
(35) Li, Z.; Jia, L.; Li, Y.; He, T.; Li, X.-M. Ammonia-Free Preparation of Ag@SiO_2 Core/Shell Nanoparticles. *Appl. Surf. Sci.* **2015**, *345*, 122−126.
(36) Oldenburg, S. J. Light Scattering from Gold Nanoshells. Ph.D. Thesis, Rice University, Houston, TX, 2000.
(37) Hsu, L.-Y.; Ding, W.; Schatz, G. C. Plasmon-Coupled Resonance Energy Transfer. *J. Phys. Chem. Lett.* **2017**, *8*, 2357−2367.
(38) Li, J.; Krasavin, A. V.; Webster, L.; Segovia, P.; Zayats, A. V.; Richards, D. Spectral Variation of Fluorescence Lifetime near Single Metal Nanoparticles. *Sci. Rep.* **2016**, *5*, 21349.
(39) Chen, Y.; Munechika, K.; Ginger, D. S. Dependence of Fluorescence Intensity on the Spectral Overlap between Fluorophores and Plasmon Resonant Single Silver Nanoparticles. *Nano Lett.* **2007**, *7*, 690−696.
(40) Lakowicz, J. R.; Shen, Y.; D'Auria, S.; Malicka, J.; Fang, J.; Gryczynski, Z.; Gryczynski, I. Radiative Decay Engineering: 2. Effects of Silver Island Films on Fluorescence Intensity, Lifetimes, and Resonance Energy Transfer. *Anal. Biochem.* **2002**, *301*, 261−277.
(41) Lakowicz, J. R.; Geddes, C. D.; Gryczynski, I.; Malicka, J.; Gryczynski, Z.; Aslan, K.; Lukomska, J.; Matveeva, E.; Zhang, J.; Badugu, R.; Huang, J. Advances in Surface-Enhanced Fluorescence. *J. Fluoresc.* **2004**, *14*, 425−441.
(42) Estrada, L. C.; Roberti, M. J.; Simoncelli, S.; Levi, V.; Aramendía, P. F.; Martínez, O. E. Detection of Low Quantum Yield Fluorophores and Improved Imaging Times Using Metallic Nanoparticles. *J. Phys. Chem. B* **2012**, *116*, 2306−2313.
(43) Theodorou, I. G.; Jawad, Z. A. R.; Jiang, Q.; Aboagye, E. O.; Porter, A. E.; Ryan, M. P.; Xie, F. Gold Nanostar Substrates for Metal-Enhanced Fluorescence through the First and Second Near-Infrared Windows. *Chem. Mater.* **2017**, *29*, 6916−6926.
(44) Kelm, A.; Waluk, J. Simulations of Fluorescence Enhancement and Emission Profile Changes in Porphyrin Attached to Gold-Silica Core-Shell Nanoparticles. *Methods Appl. Fluoresc.* **2015**, *4*, 14002.
(45) Kim, Y.; Kang, B.; Ahn, H. Y.; Seo, J.; Nam, K. T. Plasmon Enhanced Fluorescence Based on Porphyrin−Peptoid Hybridized Gold Nanoparticle Platform. *Small* **2017**, *13*, 1700071.
(46) Aroca, R. F.; Teo, G. Y.; Mohan, H.; Guerrero, A. R.; Albella, P.; Moreno, F. Plasmon-Enhanced Fluorescence and Spectral Modification in SHINEF. *J. Phys. Chem. C* **2011**, *115*, 20419−20424.
(47) Lakowicz, J. R. Radiative Decay Engineering: Biophysical and Biomedical Applications. *Anal. Biochem.* **2001**, *298*, 1−24.
(48) Geddes, C. D.; Cao, H.; Lakowicz, J. R. Enhanced Photostability of ICG in Close Proximity to Gold Colloids. *Spectrochim. Acta, Part A* **2003**, *59*, 2611−2617.
(49) Lakowicz, J. R.; Malicka, J.; Gryczynski, I. Silver Particles Enhance Emission of Fluorescent DNA Oligomers. *Biotechniques* **2003**, *34*, 62−68.
(50) Lakowicz, J. R.; Ray, K.; Chowdhury, M.; Szmacinski, H.; Fu, Y.; Zhang, J.; Nowaczyk, K. Plasmon-Controlled Fluorescence: A New Paradigm in Fluorescence Spectroscopy. *Analyst* **2008**, *133*, 1308−1346.
(51) Li, J.-F.; Li, C.-Y.; Aroca, R. F. Plasmon-Enhanced Fluorescence Spectroscopy. *Chem. Soc. Rev.* **2017**, *46*, 3962−3979.
(52) Galloway, C. M.; Artur, C.; Grand, J.; Le Ru, E. C. Photobleaching of Fluorophores on the Surface of Nanoantennas. *J. Phys. Chem. C* **2014**, *118*, 28820−28830.
(53) Vasilev, K.; Stefani, F. D.; Jacobsen, V.; Knoll, W.; Kreiter, M. Reduced Photobleaching of Chromophores Close to a Metal Surface. *J. Chem. Phys.* **2004**, *120*, 6701−6704.
(54) Tummeltshammer, C.; Brown, M. S.; Taylor, A.; Kenyon, A. J.; Papakonstantinou, I. Efficiency and Loss Mechanisms of Plasmonic Luminescent Solar Concentrators. *Opt. Express* **2013**, *21*, A735.

https://dx.doi.org/10.1021/acsaem.0c01094
ACS Appl. Energy Mater. 2020, 3, 7680−7688

(55) Slooff, L. H.; Bende, E. E.; Burgers, A. R.; Budel, T.; Pravettoni, M.; Kenny, R. P.; Dunlop, E. D.; Büchtemann, A. A Luminescent Solar Concentrator with 7.1% Power Conversion Efficiency. *Phys. Status Solidi RRL* **2008**, *2*, 257−259.
(56) Meinardi, F.; Colombo, A.; Velizhanin, K. A.; Simonutti, R.; Lorenzon, M.; Beverina, L.; Viswanatha, R.; Klimov, V. I.; Brovelli, S. Large-Area Luminescent Solar Concentrators Based on/Stokes-Shift-Engineered/' Nanocrystals in a Mass-Polymerized PMMA Matrix. *Nat. Photon.* **2014**, *8*, 392−399.
(57) Griffini, G. Host Matrix Materials for Luminescent Solar Concentrators: Recent Achievements and Forthcoming Challenges. *Front. Mater.* **2019**, *6*, 29.
(58) Jakubowski, K.; Huang, C.-S.; Gooneie, A.; Boesel, L. F.; Heuberger, M.; Hufenus, R. Luminescent Solar Concentrators Based on Melt-Spun Polymer Optical Fibers. *Mater. Des.* **2020**, *189*, 108518.
(59) Moraitis, P.; Schropp, R. E. I.; van Sark, W. G. J. H. M. Nanoparticles for Luminescent Solar Concentrators - A Review. *Opt. Mater.* **2018**, *84*, 636−645.
(60) Frias, A. R.; Pecoraro, E.; Correia, S. F. H.; Minas, L. M. G.; Bastos, A. R.; García-Revilla, S.; Balda, R.; Ribeiro, S. J. L.; André, P. S.; Carlos, L. D.; Ferreira, R. A. S. Sustainable Luminescent Solar Concentrators Based on Organic-Inorganic Hybrids Modified with Chlorophyll. *J. Mater. Chem. A* **2018**, *6*, 8712−8723.
(61) Osorio-Román, I. O.; Guerrero, A. R.; Albella, P.; Aroca, R. F. Plasmon Enhanced Fluorescence with Aggregated Shell-Isolated Nanoparticles (SHINEF). *Anal. Chem.* **2014**, *86*, 10246−10251.

https://dx.doi.org/10.1021/acsaem.0c01094
ACS Appl. Energy Mater. 2020, 3, 7680−7688